Available online at www.sciencedirect.com
SCIENCE DIRECT®
International Journal of Heat and Fluid Flow 26 (2005) 322–333
International Journal of HEAT AND FLUID FLOW
www.elsevier.com/locate/ijhff

Local heat transfer of compressible fluid in porous media: application to the HBC fuse

D. Rochette [a], S. Clain [b,*]

[a] Laboratoire Arc Electrique et Plasmas thermiques, Université Blaise Pascal, CNRS UMR 6069, Phys. Bât. 5, 24 Avenue des Landais, F 63177 Aubière Cedex, France
[b] Laboratoire Mathématiques Appliquées, Université Blaise Pascal, CNRS UMR 6620, 24 Avenue des Landais, F 63177 Aubière Cedex, France

Received 25 August 2003; accepted 4 September 2004
Available online 21 October 2004

Abstract

We propose a new model to describe compressible fluid flows in porous media introducing a microscopic thermal model to evaluate the local thermal evolution of the solid phase. Gas flow in porous media is governed by the homogenized Euler equations. We first introduce the classical non-equilibrium thermal model where the porous medium thermal distribution is driven by the heat equation. We then present the new thermal modelling introducing a characterization of the depth of the porous medium deepness. To compare the models, we have performed two critical tests: the heat exchanger and the explosion. We show that both the models agree in the first test but differ in the second case.

Keywords: Porous media; Heat transfer; Finite volume; Thermal local non-equilibrium

1. Introduction

The high breaking capacity (HBC) fuse involves heat transfer in porous media with high pressure and velocity for the gas flow (Jakubiuk and Lipski, 1993). During the discharge process (about 5 ms), a 20 000 K plasma at 10^6 Pa is generated in the fuse core and spreads in a silica sand with gas velocities up to 300 m s^{-1} (Bussière, 2001). Heat transfer between the hot gas and the porous medium warms and partially vaporizes the silica grains. Many investigations of gas flow in porous media concern heat exchange where the gas velocities are low, the temperature gradient is weak and the process is slow compared to the fuse process characteristics.

In the heat exchange, the pressure and Darcy force mainly govern the flow, the diffusion and the heat transfer mainly determine the temperature distribution. From the energy equation point of view, classical methods consider two different models in theoretical and numerical research: the local thermal equilibrium model (Jiang et al., 1999a) and the local thermal non-equilibrium model (Hsieh and Lu, 2000; Amiri and Vafai, 1994; Lee and Vafai, 1999).

The local thermal equilibrium model assumes that the solid phase temperature is equal to the gas temperature leading to an important simplification of the mathematical model. Nevertheless, the assumption of local thermal equilibrium between the gas and the solid phases is inadequate for a large number of problems. The local thermal non-equilibrium model has received considerable attention where we assume a temperature difference between the solid and the gas phases. Two equations govern the solid and the gas temperature coupled by a heat transfer term.

Both the models assume that the temperature distribution inside the particles of the porous medium is

* Corresponding author. Tel.: +33 473 407055; fax: +33 473 407064.
E-mail address: stephane.clain@math.univ-bpclermont.fr (S. Clain).

0142-727X/$ - see front matter © 2004 Elsevier Inc. All rights reserved.
doi:10.1016/j.ijheatfluidflow.2004.09.001

Nomenclature

A_0	specific surface area (m^{-1})
c_p, c_v	specific heat ($J kg^{-1} K^{-1}$)
d_p	particle diameter (m)
e	specific internal energy ($J kg^{-1}$)
E	total energy ($J m^{-3}$)
h_{sf}	heat transfer coefficient ($W m^{-2} K^{-1}$)
K	permeability (m^2)
k	thermal conductivity ($W m^{-1} K^{-1}$)
Nu	Nusselt number
p	pressure (Pa)
Pr	Prandtl number
Re	Reynolds number
T	temperature (K)
u	interstitial velocity ($m s^{-1}$)
Q	heat transfer ($W m^{-3}$)
U	vector of independent variables

Greeks

β	Forchheimer coefficient (m^{-1})
γ	adiabatique index
ϕ	porosity
μ	gas viscosity ($kg m^{-1} s^{-1}$)
ρ	density ($kg m^{-3}$)

Subscripts

g	gas
geff	effective property for gas
in	channel inlet
out	channel outlet
s	solid
seff	effective property for solid
sf	interfacial conditions

homogeneous, i.e. the peripheral temperature and core temperature of the grain are equal; but this assumption is not realistic in the case of the HBC fuse. As the classical models have failed, our specific application requires a customised model to take into account the non-homogeneous distribution of the temperature in the grain. For example, the solid grain has an important temperature gradient and its peripheral layer can reach the fusion temperature since the core remains cold. The main contribution of this present paper is to provide a modelling of the local energy distribution in the porous medium to take account of the thermal transition between the core and the surface of the grains.

A similar local heat exchange model has already been considered (Rohsenow et al., 1998) for dispersed particles in flow where we compute the thermal distribution in each sphere. Such a model considers that each particle is isolated one from the other. In the fuse case, the particles are packed and their geometry is not spherical. We thus propose a new local heat transfer model to characterize locally the temperature distribution of the porous medium by introducing a characteristic variable ξ which parameterizes the local depth in the porous medium.

The structure of the paper is as follows: in Section 2, we introduce the classical thermal non-equilibrium model comprising the Euler equations for the gas phase and the heat equation for the solid phase. We then present in Section 3 a new model to evaluate more accurately the local solid temperature distribution using a microscopic description at the pore scale and to determine the heat transfer between the two phases.

Finally, we test two characteristic situations: the heat exchange and the explosion case where we illustrate the difference between the two models.

2. The classical two-phase model

2.1. Mathematical modelling

We consider a compressible gas flowing through a one-dimensional porous medium composed of silica sand of mean radius R (see Fig. 1). Fluid flow enters the medium with a constant velocity u_0, pressure P_0 and temperature T_0 and the outflow is at atmospheric pressure.

We assume that all the functions only depend on the time t and the one-dimensional variable x. The governing equations for a single-phase fluid flow in an isotropic, homogeneous porous medium are derived from the Euler equations (Jiang and Ren, 2001; Jiang et al., 1999a).

Bear and Bachmat (1990) give the basic equations for an incompressible fluid in a porous medium and Nield (1994) gives the extension to the compressible case. The homogenization process leads us to consider three major terms: the viscous interaction between the gas and the porous medium, the heat transfer, and the momentum and thermal dispersions.

Fig. 1. Schematic diagram of a gas flowing through a porous medium.

The homogenization of the viscous term provides the Darcy force. Bear and Bachmat obtain the expression both for the isochoric and non-isochoric case (Eqs. (2.6.43) and (2.6.42) in their book). It turns out that the Darcy term is the same in both cases where an additional macroscopic viscous term is only added in the compressible case. On the other hand, in the case of a high speed flow, the laminar flow goes into a Forchheimer flow regime and a new force is added to the Darcy force to describe the fluid–structure interaction. An explicit Forchheimer force expression for incompressible fluid has been obtained by homogenization (Skjetne and Auriault, 1999; Ochoa-Tapia and Whitaker, 1998; Whitaker, 1972). In Chen et al. (2001), the authors predict that the Forchheimer law is valid even for compressible flow since it remains incompressible at a local level (De Ville, 1996).

To take into account of the thermal dispersion, Sozen and Vafai introduce in a series of papers (Alazmi and Vafai, 2000; Amiri and Vafai, 1994; Amiri et al., 1995; Sözen and Vafai, 1990; Vafai and Sözen, 1990a; Vafai and Sözen, 1990b) a diffusion term characterized by an efficient coefficient linked to the Reynolds and Prandlt numbers. The same technique is used for the momentum dispersion where Bear and Bachmat (1990) propose an artificial viscosity for isochoric flow characterized by a mechanical dispersion coefficient linked to the Peclet number. For the turbulent gas with dispersed particles, Simonin (1991) uses the artificial viscosity concept taking account of the turbulent fluid motion on a large scale with a $q^2-\epsilon$ model (Balzer et al., 1995).

Finally, a source term depending on the temperature difference between the two media is added to the fluid and porous medium energy equations to describe the heat transfer between the fluid and the porous medium. Several correlations are proposed to determine the heat transfer coefficient depending on the Reynolds, Nusselt and Prandlt numbers.

In the present paper, we neglect the macroscopic viscous term and the momentum dispersion term since the fluid is essentially governed by the convection and the pressure. On the other hand, we characterize the thermal dispersion using a diffusion operator (Amiri and Vafai, 1994) in order to measure its impact on the thermal model. Consequently, the considered model takes the form:

$$\frac{\partial(\rho_g\phi)}{\partial t}+\frac{\partial(\rho_g\phi u)}{\partial x}=0, \tag{1}$$

$$\frac{\partial(\rho_g\phi u)}{\partial t}+\frac{\partial(\rho_g\phi u^2+\phi P)}{\partial x}=-\phi^2\frac{\mu}{K}u-\phi^3\beta\rho_g\mid u\mid u, \tag{2}$$

$$\frac{\partial(\phi E)}{\partial t}+\frac{\partial[(E+P).\phi u]}{\partial x}=\frac{\partial}{\partial x}\left(k_{geff}\frac{\partial T_g}{\partial x}\right)-Q, \tag{3}$$

where ρ_g is the gas density, u the interstitial velocity, P the pressure and ϕ the porosity. Note that we keep the advective and the inertial terms in the momentum equation leading to a hyperbolic system. In low velocity flow, such terms are omitted (Alazmi and Vafai, 2000; Amiri and Vafai, 1994). On the right-hand side, the mechanical interaction is represented by the viscous force (Darcy law), with K the permeability and μ the gas viscosity and the inertial resistance (Forchheimer law) where β is the forchheimer coefficient (Macdonald et al., 1979; Teng and Zhao, 2000; Whitaker, 1996). In the energy conservation equation, E is the gas total energy per unit volume and e is the specific internal energy:

$$E=\rho_g\left(\frac{1}{2}u^2+e\right)\quad\text{with}\quad e=c_vT_g,$$

where c_v is the gas specific heat coefficient at constant volume and T_g is the gas temperature. In addition, to close the system of equations, we use the ideal gas equation of state

$$P(\rho,e)=(\gamma-1)\rho_g e\quad\text{with}\quad\gamma>1, \tag{4}$$

where γ is the ratio of specific heat coefficients of the gas. Ishii (1975) presents a general method to get the state equation. Eq. (4) is not correct with the averaged values since additional terms like the turbulent kinetic energy appear with the averaged process. But, if we neglect the fluctuating moments in comparison with the averaged values, we conclude that state equation relation (4) with the averaged variables is a rather good approximation.

The thermal diffusion is driven by the gas phase effective thermal coefficient k_{geff} given by the empirical correlation of Amiri and Vafai (1994):

$$k_{geff}=\phi k_g+0.5\left[Pr\left(\frac{\rho u d_p}{\mu}\right)\right]k_g. \tag{5}$$

The thermal interaction $Q=h_{sf}A_0(T_g-T_s)$ between the gas and the solid grains is governed by an empirical law (Rohsenow et al., 1998) which depends on the convective heat transfer coefficient h_{sf}, the specific interface surface area per unit volume $A_0=6(1-\phi)/d_p$ (Jiang and Ren, 2001) where d_p is the particle diameter, and the gas and solid temperatures. The convective heat transfer coefficient h_{sf} has been determined experimentally by various authors. Wakao and Kaguei (1982) (see also Achenbach, 1995) propose a correlation in the case of packed spheres:

$$h_{sf}=\frac{k_g}{d_p}(2+1.1Re^{0.6}Pr^{1/3}). \tag{6}$$

Other correlations are used, for example Alazmi and Vafai (2000) propose

$$h_{sf} = \left[\frac{d_p \phi}{0.2555 Pr^{1/3} Re^{2/3} k_g} + \frac{d_p}{10 k_g} \right]^{-1}, \quad (7)$$

where $Nu = h_{sf} d_p / k_g$, $Re = \rho_g \phi u d_p / \mu$ and $Pr = \mu c_{pg} / k_g$ are respectively the Nusselt, Reynolds and Prandlt numbers, k_g is the gas thermal conductivity. We can notice that for large Reynolds numbers, all the expressions give the same heat transfer coefficient. The correlations only differ for low Reynolds numbers.

Finally, to model the heat transfer process between the gas and solid phases, we introduce the classical heat equation with a longitudinal thermal conduction in the solid phase (Bortolozzi and Deiber, 2001) to evaluate the solid temperature distribution T_s:

$$\rho_s c_{vs} \frac{\partial T_s}{\partial t} = \frac{k_{seff}}{(1-\phi)} \frac{\partial^2 T_s}{\partial x^2} + \frac{Q}{(1-\phi)}, \quad (8)$$

where ρ_s denotes the solid density, c_{vs} is the solid specific heat at constant volume and k_{seff} is the porous medium conductivity with $k_{seff} = (1-\phi) k_s$.

2.2. Discretization schemes and numerical method

At time $t = 0$, we assume that the gas is at rest, the pressure is atmospheric and the temperatures (solid and gas) are equal to 300 K. For $t > 0$, we inject a hot gas with a temperature T_0, a pressure P_0 and a velocity u_0 at $x = 0$. On the other hand, we prescribe at $x = L$ an atmospheric pressure outflow.

Most authors use the method of finite differences since they do not take the advective term into account. In the present case, we use a finite volume scheme to solve numerically the gas system (Eqs. (1)–(3)). The motivation is to provide a correct resolution of the hyperbolic system without adding any artificial viscosity to stabilize the scheme. We write the system in the conservative form (Toro, 1997):

$$\frac{\partial U}{\partial t} + \frac{\partial F(U)}{\partial x} = S(U), \quad (9)$$

where U is the conservative variable vector and $F(U)$, $S(U)$ are respectively the flux vector and the source vector in function of vector U and the fixed parameters:

$$U = \begin{pmatrix} \rho_g \phi \\ \rho_g \phi u \\ \phi E \end{pmatrix}, \quad F(U) = \begin{pmatrix} \rho_g \phi u \\ \rho_g \phi u^2 + \phi P \\ (E+P) \phi u \end{pmatrix},$$

$$S(U) = \begin{pmatrix} 0 \\ -\phi^2 \frac{\mu}{K} u - \phi^3 \beta \rho_g \mid u \mid u \\ \frac{\partial}{\partial x} \left(k_{geff} \frac{\partial T_g}{\partial x} \right) - h_{sf} A_0 (T_g - T_s) \end{pmatrix}.$$

2.2.1. The fractional step technique

In order to obtain an approximate solution of system (9), we use a fractional step technique (Ben-Dor et al., 1997; Rochette and Clain, 2003; Rochette and Clain, 2004): for a given time interval $[t^n, t^{n+1}]$, we first solve the homogeneous conservative system and then the right-hand side terms. More precisely, let U^n be an approximation of $U(t^n)$ at time t^n, in order to obtain an approximation of $U(t^{n+1})$ at time $t^{n+1} = t^n + \Delta t$, we first determine an approximate solution over the time interval $[t^n, t^{n+1}]$ of the homogeneous problem

$$\begin{cases} \frac{\partial U}{\partial t} + \frac{\partial F(U)}{\partial x} = 0, \\ U(x, t^n) = U^n, \end{cases} \quad (10)$$

using the finite volume scheme presented in Section 2.2.2. Let us now assume that $\widetilde{U}^{n+1}$ is the approximate solution value at $t = t^{n+1}$ of Eq. (10), we solve the ordinary differential equation

$$\frac{dU}{dt} = S(U), \quad (11)$$

using $\widetilde{U}^{n+1}$ as initial condition at $t = t^n$. The solution at $t = t^{n+1}$ of Eq. (11) is an approximation U^{n+1} of $U(t^{n+1})$.

2.2.2. The homogeneous and source problems

We briefly describe the finite volume method based on a Roe's solver (Roe, 1981). Let us consider a uniform grid of the porous domain $[0, L]$ setting $x_i = (i - \frac{1}{2})\Delta x$ with $i = 1 \ldots N$, and

$$x_{i-1/2} = x_i - \frac{\Delta x}{2}, \quad x_{i+1/2} = x_i + \frac{\Delta x}{2}.$$

For each index i, $C_i = [x_{i-1/2}, x_{i+1/2}]$ represents the cell of center x_i and length Δx. Assuming that we know an approximation $U_i^n = ((\rho_g \phi)_i^n, (\rho_g \phi u)_i^n, (E\phi)_i^n)$ of $U(x_i, t^n)$ at the time t^n on each cell C_i, we seek an approximation $\widetilde{U}^{n+1}$ for the homogeneous problem (10) using an explicit finite volume scheme of the form

$$\widetilde{U}_i^{n+1} = U_i^n - \frac{\Delta t_h}{\Delta x} (F_{i+1/2}^n - F_{i-1/2}^n), \quad (12)$$

where $F_{i+1/2}^n$ and $F_{i-1/2}^n$ represent respectively the numerical fluxes calculated at the interface cells $x = x_{i+1/2}$ and $x = x_{i-1/2}$ using the Roe's solver. We reach second order spatial accuracy using the MUSCL method with slope limited (Yee, 1987; Abgrall, 1988). Moreover, the time step Δt_h is chosen in agreement with the Courant–Friedrichs–Lewy (CFL) condition (Courant and Friedrichs, 1948).

The second step consists in solving the first-order system of ordinary differential equations (Toro, 1997):

$$\frac{dU}{dt} = \begin{pmatrix} 0 \\ -\phi^2 \frac{\mu}{k} u - \phi^3 \beta \rho_g \mid u \mid u \\ -h_{sf} A_0 (T_g - T_s) \end{pmatrix}. \quad (13)$$

Numerically, we use a fourth-order explicit Runge–Kutta method. Since the method is explicit, a stability condition arises and the time step Δt must be lower than a

limiting time interval Δt_l. Finally, we add the diffusion contribution by:

$$\rho_g c_{pg} T^{n+1}_{g,i} = \rho_g c_{pg} T^{n}_{g,i} + \frac{\Delta t_d}{\Delta x}(f^n_{i+1/2} - f^n_{i-1/2}), \quad (14)$$

where Δt_d is the time step of the diffusion term such that $\Delta t_d < \rho_g c_{pg}(\Delta x)^2/k_{geff}$ to satisfy the stability condition of the explicit scheme. The computation of $f^n_{i+1/2}$, $f^n_{i-1/2}$ is detailed in the next section.

2.2.3. Solid energy equation

To compute the temperature in the solid, we consider the same uniform grid of the domain $[0, L]$. Assuming that we know an approximation $T^n_{s,i}$ of $T_s(x_i, t^n)$ at t^n on the cell C_i, we seek an approximate $T^{n+1}_{s,i}$ at time t^{n+1} using an explicit finite volume method given by:

$$\rho_s c_{vs} T^{n+1}_{s,i} = \rho_s c_{vs} T^{n}_{s,i} + \frac{\Delta t_s}{\Delta x}(f^n_{i+1/2} - f^n_{i-1/2}) + \Delta t_s h^n_{sf,i} A_0 (T^n_{g,i} - T^n_{s,i}), \quad (15)$$

where central differences are used to determine the fluxes, i.e.:

$$f^n_{i+1/2} = k_{seff}\frac{T^n_{s,i+1} - T^n_{s,i}}{\Delta x} \quad \text{and} \quad f^n_{i-1/2} = k_{seff}\frac{T^n_{s,i} - T^n_{s,i-1}}{\Delta x}.$$

The explicit scheme is stable if we satisfy the condition $\Delta t_s < \rho_s c_{vs}(\Delta x)^2/k_{seff}$ but in practice, the CFL condition for the gas flow problem gives a more restrictive condition than the stability condition. Therefore an implicit scheme is not necessary.

2.2.4. The numerical treatment of the boundary conditions

Boundary conditions are necessary to complete the flux contribution on the interfaces $x = 0$ and $x = L$. We add fictitious cells C_0 and C_{N+1} where we prescribe the boundary conditions (Toro, 1997). For the C_0 cell, we set the inflow conditions

Table 1
Input data used in the numerical calculation

Porosity	$\phi = 0.4$
Permeability	$K = 6 \times 10^{-11}\,\mathrm{m}^2$
Forchheimer coefficient	$\beta = 3.3 \times 10^4\,\mathrm{m}^{-1}$
Grain diameter	$d_p = 3 \times 10^{-4}\,\mathrm{m}$
Viscosity	$\mu = 1.8 \times 10^{-5}\,\mathrm{kg\,m^{-1}\,s^{-1}}$
Gas thermal conductivity	$k_g = 0.026\,\mathrm{W\,m^{-1}\,K^{-1}}$
Porous media thermal conductivity	$k_{seff} = 0.33\,\mathrm{W\,m^{-1}\,K^{-1}}$
Ratio of specific heat	$\gamma = 1.4$
Solid specific heat at constant volume	$c_{vs} = 1420.74\,\mathrm{J\,kg^{-1}\,K^{-1}}$

$$U^n_0 = \begin{pmatrix} (\rho_g\phi)^n_0 \\ (\rho_g\phi u)^n_0 \\ (E\phi)^n_0 \end{pmatrix},$$

and for the C_{N+1} cell, we set the outflow conditions under the assumption that the outside pressure is atmospheric

$$U^n_{N+1} = \begin{pmatrix} (\rho_g\phi)^n_{N+1} \\ (\rho_g\phi u)^n_{N+1} \\ (E\phi)^n_{N+1} \end{pmatrix} = \begin{pmatrix} (\rho_g\phi)^n_N \\ (\rho_g\phi u)^n_N \\ \frac{P_{atm}}{(\gamma-1)} + \frac{1}{2}(\rho_g\phi u)^n_N u^n_N \end{pmatrix}.$$

2.3. Convergence tests

We consider a 0.1 m size domain filled with a porous medium composed of silica sand. We inject a constant gas mass flux $(\rho_g\phi u)^n_0 = 25\,\mathrm{kg\,m^{-2}\,s^{-1}}$ with a temperature of $(T_g)_0 = 1160\,\mathrm{K}$ during $t = 1\,\mathrm{s}$. At the initial time $t = 0$, the system is at rest, $u = 0\,\mathrm{m\,s^{-1}}$, the gas present in the porous medium interstices is at atmospheric pressure and ambient temperature $T_g = T_s = 300\,\mathrm{K}$. The gas and the porous medium parameters used in the numerical simulations are shown in Table 1.

In order to compare the two models and for the sake of simplicity, we have used constant coefficients. The numerical solver of the gas system has been tested in a similar situation in Rochette and Clain (2004) where

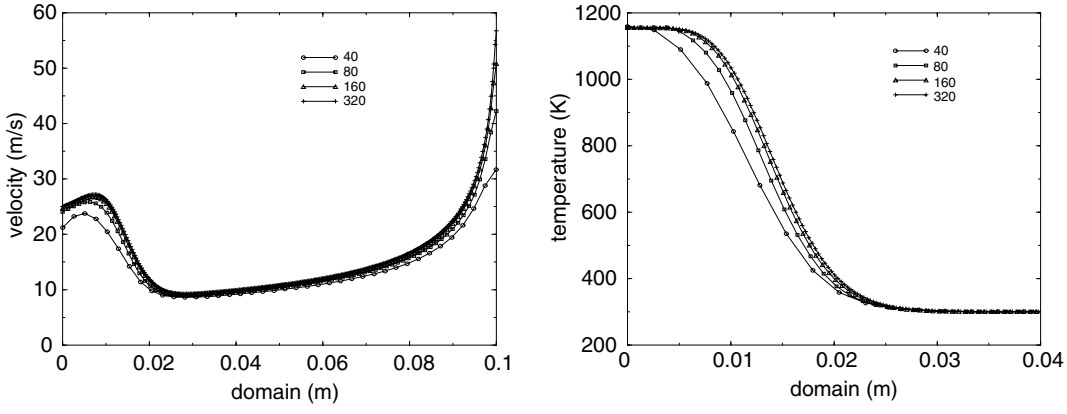

Fig. 2. Velocity and temperature distribution in the porous medium domain at $t = 1$ s for several meshes.

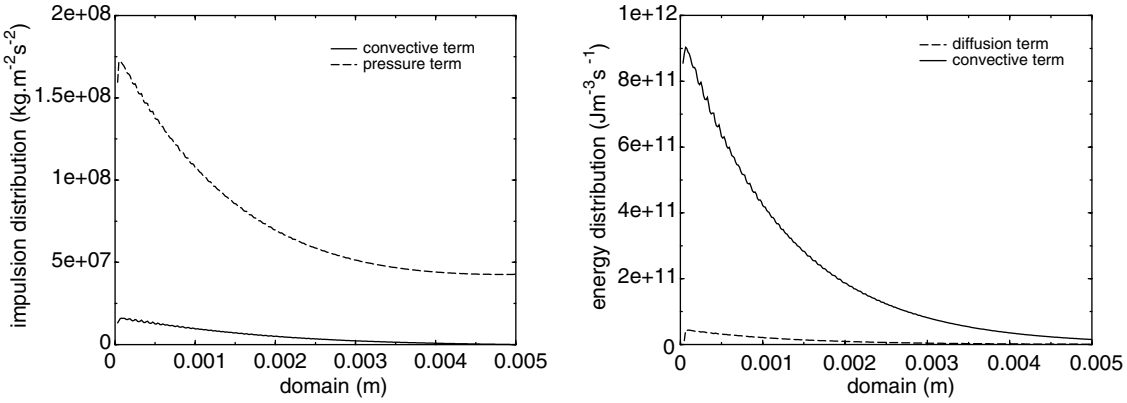

Fig. 3. (left) Comparison of the convective and pressure forces at $t = 5$ ms. (right) Comparison of the energy convection and energy diffusion at $t = 5$ ms.

we present a convergence test based on a stationary solution. All the computations have been performed with a C++ code using a dedicated Object Finite Element LIbrary OFELI (Touzani, 1998).

We present simulation results with four meshes composed of 40, 80, 160 and 320 uniform cells respectively. Fig. 2 represents the evolution of the gas velocity and gas temperature in the domain after 1 s. For the four different meshes, the results are similar with a significant difference between 40 and 320 cells close to the boundaries. The stability condition involves four time steps Δt_h, Δt_l, Δt_d and Δt_s, so we choose a time step Δt lower than $\min(\Delta t_h, \Delta t_l, \Delta t_d, \Delta t_s)$. In our application, the minimum is the homogeneous time step Δt_h.

We note that for a mesh of 80 cells, the convergence is sufficient in comparison with a mesh of 320 cells and in the sequel, we will use an 80 cell mesh to reduce the time computation. Another remark is the high mesh sensibility of the outflow velocity to respect the outside atmospheric pressure condition. Fortunately, it has a low impact from the energy point of view. We shall use this benchmark to compare the numerical solution of the micro/macro model presented in the Section 3.

2.4. Simulations and justifications

A first set of simulations has been performed to compare the correlations used to characterize the heat transfer. For the same initial conditions given in the previous section, we run the program with both the Wakao and Kaguei (1982) (Eq. (6)) formula and the correlation proposed by Alazmi and Vafai (2000) (Eq. (7)). We do not present any curve since we obtain the same thermal distributions. Indeed, the relations give the same heat transfer coefficient for high Reynolds numbers (i.e. $Re \geqslant 300$) and the heat transfer contribution is negligible for low Reynolds numbers. Consequently, we shall use the Wakao and Kaguei (1982) formula in the sequel.

Most authors do not consider the convection term in the momentum equation since the pressure forces is greater than the convection force. This is realistic for the heat exchanger case. We compare here the convective term $\partial(\rho u^2)/\partial x$ and the pressure $\partial p/\partial x$ forces and compute their contributions. In a first run, we use the initial and boundary conditions of the previous section. We obtain velocity flow higher than $20\,\mathrm{m\,s^{-1}}$. In this case, the convective term represents less than 1% of the pressure force and can be neglected. We perform a second run using boundary conditions such that we obtain a gas velocity of about $200\,\mathrm{m\,s^{-1}}$ which is realistic for the HBC fuses. In this case, the convective contribution is greater than 10% of the pressure force and should not be omitted (see Fig. 3). We proceed in the same way to evaluate the thermal diffusion contribution and compare the numerical values of the convective part $\partial(u(E+p))/\partial x$ with the diffusion part $\partial(k_{\mathrm{geff}}\partial T_g/\partial x)/\partial x$. In the first run (low velocity), the result is that the diffusion is smaller (<1%) than the convective part. We have also run the code without the diffusion and the temperature, velocity and pressure are the same. In the second run (high velocity), we get that the diffusion contribution is about 5% (see Fig. 3).

3. The Macroscopic model with a microscopic 2D approach

As we have emphasized in the introduction, the temperature inside the grain is not homogeneous, which leads us to consider a new model in which we predict the temperature distribution in the grains. A first idea consists of representing the grain by a sphere of radius R and solving the heat equation adding some flux condition on the boundary as Rohsenow et al. (1998), Section 9.34. This model is correct if the spheres (i.e. the grains) are isolated from one another, but in the HBC fuse (or any packed porous medium), the grains are in contact and their geometry is not spherical, therefore the sphere model is inapplicable. To model the heat distribution in the grains, we introduce a characteristic variable ξ such

that $\xi = 0$ corresponds to the center of the grain and $\xi = l_1$ to the boundary where we shall set the l_1 value in the sequel. At any point x, we give a local description of the solid temperature with a temperature $\theta_s(x,\xi)$ governed by the heat equation:

$$\frac{\partial \epsilon_s}{\partial t} - \frac{\partial}{\partial \xi}\left(k_s \frac{\partial \theta_s}{\partial \xi}\right) = 0, \quad \text{in} \quad 0 < \xi < l_1, \tag{16}$$

where ϵ_s and k_s denote respectively the solid internal energy and the solid thermal conductivity.

To take into account the thermal diffusion of the grain arising from the grain–grain contact, we complete Eq. (16) with the diffusion term following the x-direction:

$$\frac{\partial \epsilon_s}{\partial t} - \frac{\partial}{\partial x}\left(k_s \frac{\partial \theta_s}{\partial x}\right) - \frac{\partial}{\partial \xi}\left(k_s \frac{\partial \theta_s}{\partial \xi}\right) = 0, \quad \text{in} \quad 0 < x < L, \quad 0 < \xi < l_1. \tag{17}$$

The rectangular domain $\Omega =]0.L[\times]0, l_1[$ represents the domain of the porous media such that the x-direction is the macroscopic distribution in the fuse and the ξ-direction is the microscopic distribution in the grain.

We close the model by adding the one-dimensional gas equations of the mass, momentum and energy conservation:

$$\frac{\partial(\rho_g \phi)}{\partial t} + \frac{\partial(\rho_g \phi u)}{\partial x} = 0, \tag{18}$$

$$\frac{\partial(\rho_g \phi u)}{\partial t} + \frac{\partial(\rho_g \phi u^2 + \phi P)}{\partial x} = -\phi^2 \frac{\mu}{K} u - \phi^3 \beta \rho_g \mid u \mid u, \tag{19}$$

$$\frac{\partial(E\phi)}{\partial t} + \frac{\partial[\phi u(E+P)]}{\partial x} = -Q + \frac{\partial}{\partial x}\left(k_{geff} \frac{\partial T_g}{\partial x}\right). \tag{20}$$

To evaluate the heat source term Q in the gas, we use the same experimental correlation, i.e.

$$Q = h_{sf} A_0 (T_g(x) - \theta_s(x, l_1)), \tag{21}$$

where $\theta_s(x, l_1)$ is the temperature at the surface grains.

In the solid, we impose the condition $\partial\theta_s/\partial x = 0$ at $\xi = 0$ due to the symmetry at the grain center. At the fluid–solid interface, we set the Neumann condition:

$$k_s \frac{\partial \theta_s}{\xi} = l_2 Q, \tag{22}$$

to describe the heat transfer. To characterize l_1 and l_2, we integrate Eq. (17) as a function of ξ and we get with the boundary conditions:

$$\frac{\partial}{\partial t}\int_0^{l_1} \epsilon_s \mathrm{d}\xi - \frac{\partial}{\partial x}\left(k_s \frac{\partial}{\partial x}\left(\int_0^{l_1} \theta_s \mathrm{d}\xi\right)\right) = l_2 Q. \tag{23}$$

Assuming that we reach the thermally homogeneous case (i.e. ϵ_s and θ_s do not depend on ξ), we have $\epsilon_s(x,\xi) = e_s(x) = c_{vs} T_s(x)$ and $\theta_s(x,\xi) = T_s(x)$ and Eq. (23) yields:

$$\frac{\partial e_s}{\partial t} - \frac{\partial}{\partial x}\left(k_s \frac{\partial T_s}{\partial x}\right) = Q \frac{l_2}{l_1}. \tag{24}$$

In comparison with Eq. (8), we have $l_1 = (1-\phi) l_2$ where l_2 is the characteristic length of the porous medium and we get $k_{seff} = (1-\phi) k_s$. In our case, we choose the grain mean radius R for l_2.

3.1. Numerical method

The numerical method is based on a fractional step technique. Assuming that we know approximations ρ_g^n, u^n, E^n and T_g^n for the gas at time t^n and θ_s^n, ϵ_s^n for the solid and let Δt be a small time interval.

- We first compute an approximation of the flux Q^n between the gas and the solid phase.
- Secondly, we compute an approximation ρ_g^{n+1}, u^{n+1}, E^{n+1} and T_g^{n+1} solving Eqs. (18)–(20) using the fractional step method described in Section (2.2.2).
- Finally, we solve the heat equation in the solid domain adding at the solid–gas interface the flux Q to obtain ϵ_s^{n+1} and θ_s^{n+1} using a finite volume method as presented in the next section.

3.2. The heat equation resolution

We consider a two-dimensional mesh composed of rectangular cells. For each cell, x_j, ξ_j denote the cell center coordinates of length Δx and height $\Delta\xi$. Since we have to handle two meshes, the one-dimensional mesh for the gas and the two-dimensional mesh for the porous media, we impose a mesh compatibility such that each 2D mesh column corresponds to a 1D cell (see Fig. 4).

The computation is based on an implicit finite volume scheme. Indeed, an explicit scheme requires the use of very small time steps to satisfy the stability condition

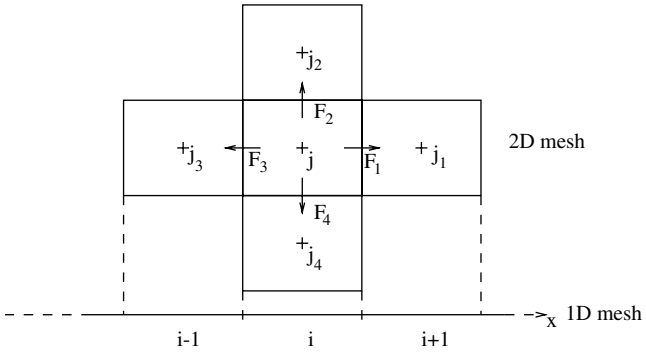

Fig. 4. The control volumes.

because $\Delta\xi$ is very small which leads to unrealistic computation times.

The implicit formulation is given by:

$$\rho_s c_{vs}\theta_{s,j}^{n+1} = \rho_s c_{vs}\theta_{s,j}^{n} + \frac{\Delta t}{\Delta x}(F_1^{n+1} - F_3^{n+1}) + \frac{\Delta t}{\Delta \xi}(F_2^{n+1} - F_4^{n+1}), \quad (25)$$

where F_1, F_2, F_3 and F_4 represent the numerical fluxes at the cell interfaces using a centered difference scheme:

$$\begin{aligned}\rho_s c_{vs}\theta_{s,j}^{n+1} = {} & \rho_s c_{vs}\theta_{s,j}^{n} + 2\Delta t k_{j,j_1}(\theta_{s,j_1}^{n+1} - \theta_{s,j}^{n+1})\frac{(l_{j,j_1})^2}{S_j(S_j + S_{j_1})} \\ & - 2\Delta t k_{j,j_3}(\theta_{s,j_3}^{n+1} - \theta_{s,j}^{n+1})\frac{(l_{j,j_3})^2}{S_j(S_j + S_{j_3})} \\ & + 2\Delta t k_{j,j_2}(\theta_{s,j_2}^{n+1} - \theta_{s,j}^{n+1})\frac{(l_{j,j_2})^2}{S_j(S_j + S_{j_2})} \\ & - 2\Delta t k_{j,j_4}(\theta_{s,j_4}^{n+1} - \theta_{s,j}^{n+1})\frac{(l_{j,j_4})^2}{S_j(S_j + S_{j_4})}, \end{aligned} \quad (26)$$

where l_{jk}, $k = j_1, j_2, j_3, j_4$ represents the length between the cells and S_j the j cell surface.

Due to the boundary condition assumption, we take the flux equal to zero at $x = 0$, $x = L$, $\xi = 0$. At $\xi = l_1$, we set $F_2 = l_2 h_{sf} A_0(T_{g,i}^n - \theta_{s,j}^n)$ where the cell j is the upper 2D mesh cell of the column i which correspond to the 1D cell i.

The discretized heat equation is rewritten in the matrix form:

$$A\theta_s^{n+1} = B(\theta_s^n), \quad (27)$$

where A is a symmetrical matrix since we have a regular mesh. We obtain θ_s^{n+1} solving the linear system Eq. (27) by a conjugated gradient method.

3.3. Convergence test

To test the convergence of the numerical scheme, we use an 80 cell mesh following the x-direction and four discretizations of 10, 20, 40 and 80 cells following the ξ-direction to see the mesh dependence on the heat transfer between the gas and the solid (Fig. 5). The initial and boundary conditions are identical to the ones prescribed in the previous section.

Numerical simulations show that we obtain a good stability result for an 80×80 cell mesh and the numerical solutions converge to a limite as we refine the mesh.

4. Comparison of the two models

We compare the models in two characteristic situations: the first one consists of slowly heating a porous medium for 1 s and the second one consists of quickly heating the porous medium for 5 ms to highlight the difference between the two models. In the following calculations, we use the sand grain characteristics: $l_1 = 180\,\mu m$, $k_s = 1.8\,W\,m^{-1}\,K^{-1}$, $c_p = 1420\,J\,kg^{-1}\,K^{-1}$ and $\rho = 2650\,kg\,m^{-3}$.

4.1. Heat exchanger simulation

A constant mass flux $(\rho_g \phi u)_0 = 25\,kg\,m^{-2}\,s^{-1}$ at temperature $(T_g)_0 = 1180\,K$ enters for 1 s into the porous medium at $x = 0$. We compare the evolution of the velocity, density, gas and solid temperatures for the two models. For the 1-model, we have used an 80-cell mesh and for the 2-model a 80×80 cell mesh.

Fig. 6 presents the comparison of the velocity and the density distributions for the gas between the two models at $t = 1$ s. We observe that the velocity and density profiles calculated with the two models almost coincide. Fig. 7 presents the comparison of the gas temperature and the solid temperature distributions at $t = 1$ s. For the 2-model, we show the temperature interface at $\xi = l_1$ and the temperature core at $\xi = 0$ in a sand grain. We observe that the solid temperature is homogeneous, i.e. the interface and core temperatures are equal. In this case, the gas and the solid phases are in thermal

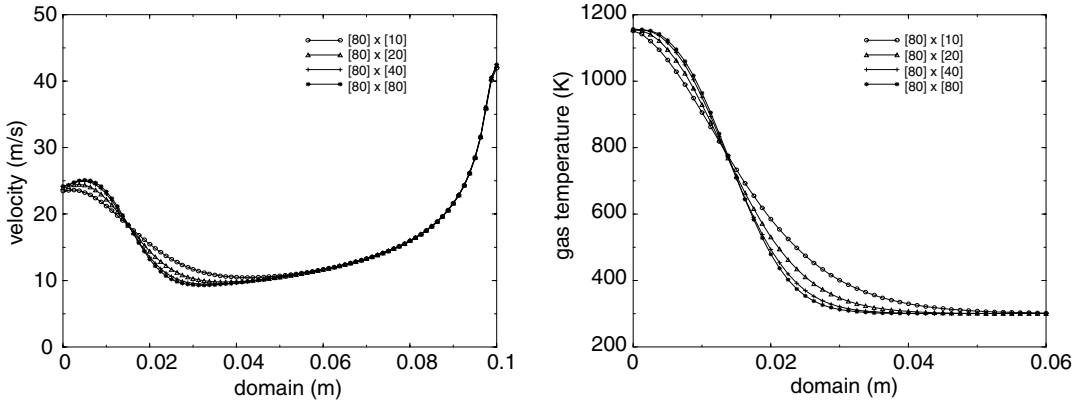

Fig. 5. Velocity and temperature distributions in the porous medium domain at $t = 1$ s for several meshes.

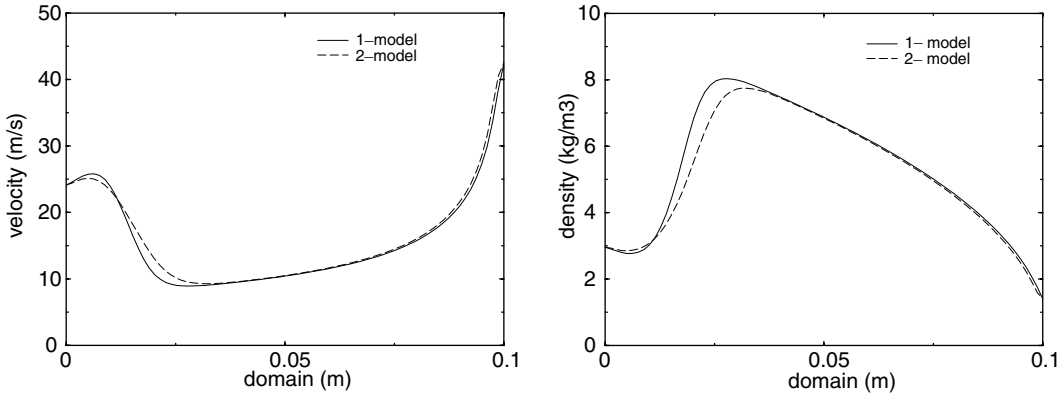

Fig. 6. Comparison of velocity and density distributions in the porous medium domain at $t = 1\,\mathrm{s}$.

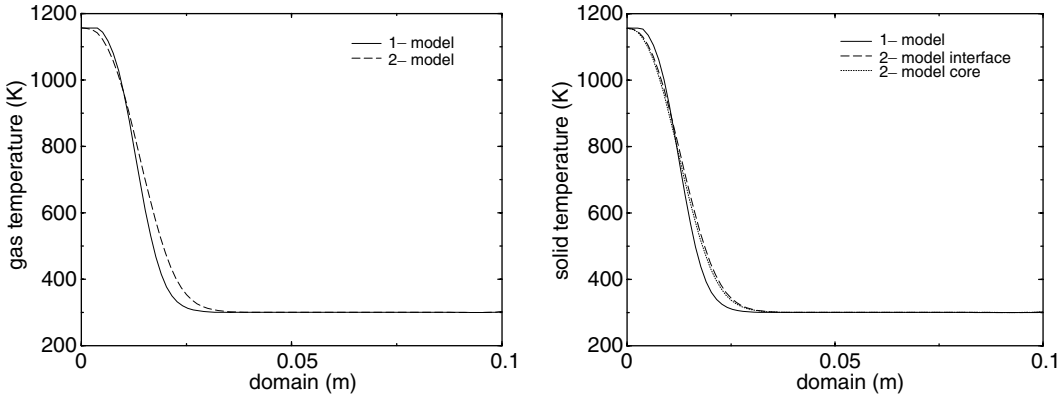

Fig. 7. Comparison of the gas and the solid temperature distributions in the porous medium domain at $t = 1\,\mathrm{s}$.

equilibrium $T_g \approx \theta_s$ for the two models and we note that the curves are similar with a slight difference in the heat transfer zone. The difference derives from the small temperature difference between the core and the interface grain. The surface temperature is a somewhat greater than the temperature in the first model and the heat transfer is less important: we transport the energy for a little longer.

4.2. The HBC fuse simulation (5 ms)

The second test concerns the explosive case. A constant inlet flux of gas is injected into the porous medium with $(\rho_g \phi u)_0 = 70\,\mathrm{kg\,m^{-2}s^{-1}}$ and a gas temperature of $(T_g)_0 = 3000\,\mathrm{K}$. Computations have been performed for a period of 5 ms with a $L = 10\,\mathrm{mm}$ domain length.

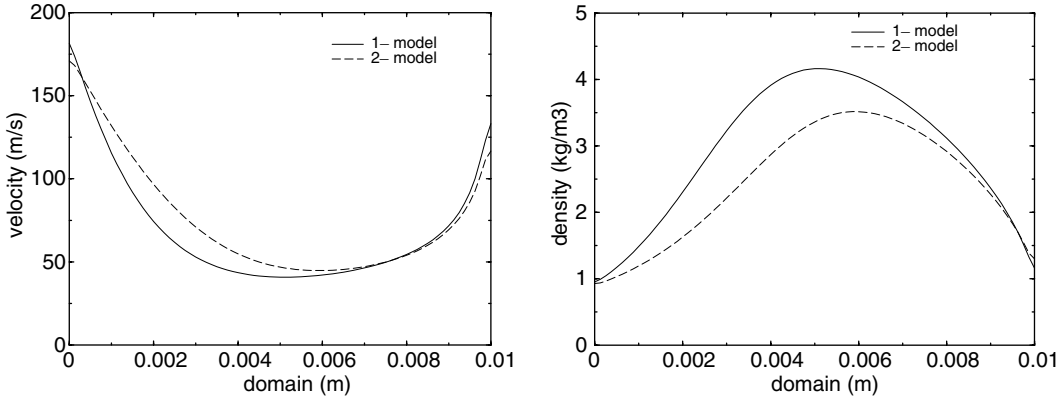

Fig. 8. Comparison of the velocity and density distributions in the porous medium domain at $t = 5\,\mathrm{ms}$ between the two models.

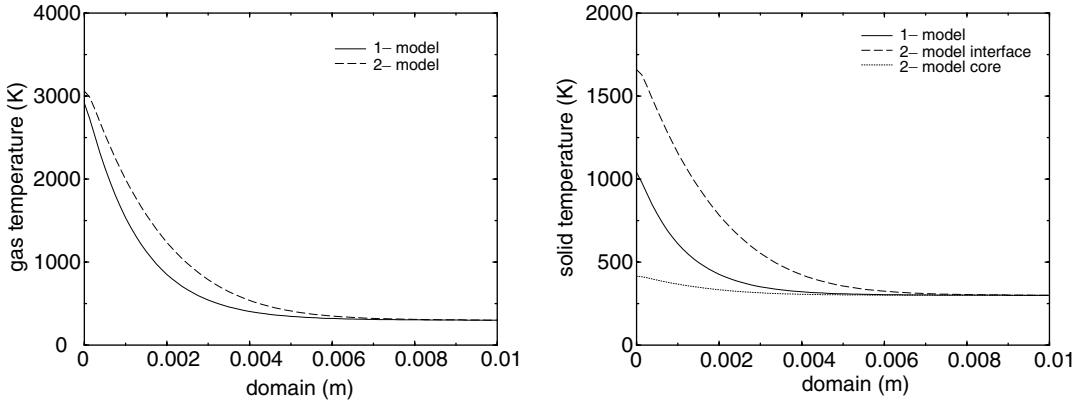

Fig. 9. Comparison of the gas and solid temperature distributions in the porous medium domain at $t = 5$ ms between the two models.

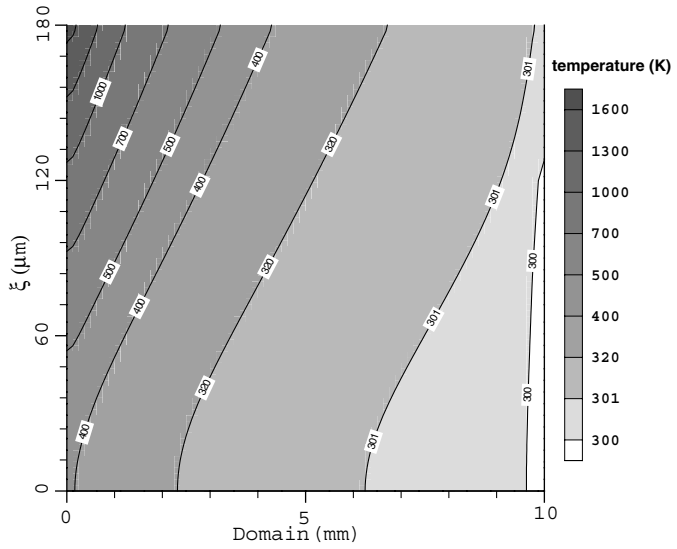

Fig. 10. Temperature distribution in the porous medium following x-direction and in the sand grains following the ξ-direction at time $t = 5$ ms.

Fig. 8 presents the velocity and density of the gas obtained from the two models at $t = 5$ ms. In this particular situation, the velocity and density profiles of the 2-model are different from the 1-model. The mechanical effect of the gas flow is also modified, in particular the Darcy and Forchheimer force distribution. Fig. 9(left) presents the comparison of the gas temperature and the Fig. 9(right) presents the solid temperature obtained from the 1-model and the interface, core solid temperatures of the 2-model. The heat transfer with the 1-model is greater than that with the 2-model. As explained in the previous section, the energy is transported further since the heat transfer is lower in the 2-model than the 1-model. This numerical experiment shows that the solid homogeneous temperature assumption is no longer valid. The interface and the core temperature inside a grain are dramatically different since we obtain an interface temperature of around 1650 K while the core temperature is 420 K.

Fig. 10 represents the temperature distribution in the porous medium at time $t = 5$ ms. The ξ-direction gives the distribution in the grain for any fixed x. We obtain a large temperature differential at $x = 0$ which confirms the non-homogeneous distribution of the energy inside the grains and modifies the heat transfer. This phenomenon occurs during the fuse operation process where the first grains are partially vaporized.

5. Conclusion

In this paper, we have proposed a new modelling of a compressible gas flow in porous media based on a microscopic description of the heat transfer between the two-phases. We have used a one-dimensional gas flow model in porous media taking into account the mechanical interaction between the gas and the porous medium. To evaluate the heat transfer between the

two phases, we have introduced a two-dimensional local heat transfer model depending on the characteristic length l_1 of the medium.

Numerical simulations using a fractional step technique and a finite volume method have been performed to evaluate the solid temperature distribution in silica sand grains. We have compared the model with a classical thermal non-equilibrium homogenized model for two characteristic situations. We have shown that the two models agree when the gas inflow velocity is low and when the simulation time is long. However, for the explosion situation, the assumption that we have a solid homogeneous temperature does not hold when the diffusion into the solid is less rapid than the whole process duration. The 1-model is computationally less costly and should be used in the case of a homogeneous temperature distribution in the grain. The 2-model only has to be considered when the temperature gradient is important, in particular when the vaporization process occurs. In this case, the thermal distribution will be helpful to determine the vaporization rate.

Acknowledgements

The authors would like to thank F. Gentils of Schneider Electric, X. Godechot and S. Melquiond of Alstom, M.R. Rambaud of Ferraz S.A. for their financial support. We also thank T. Buffard for many discussions in the field of the numerical simulations and R. Touzani for his advice the on OFELI library.

References

Abgrall, R., 1988. Generalisation of the Roe scheme for the computation of mixture of perfect gases. La Recherche Aérospatiale 6, 31–43.

Achenbach, E., 1995. Heat and flow characteristics of packed beds. Experimental Thermal and Fluid Science 10, 17–27.

Alazmi, B., Vafai, K., 2000. Analysis of variants within the porous media transport models. ASME Journal of Heat Transfer 122, 303–326.

Amiri, A., Vafai, K., 1994. Analysis of dispersion effects and non-thermal equilibrium, non-Darcian, variable porosity incompressible flow through porous medium. International Journal of Heat and Mass Transfer 37, 939–954.

Amiri, A., Vafai, K., Kuzay, T.M., 1995. Effects of boundary conditions on non-darcian heat transfer through porous media and experimental comparisons. Numerical Heat Transfer, Part A 27, 651–664.

Balzer, G., Boelle, A., Simonin, O., 1995. Eulerian gas–solid flow modelling of dense fluidized bed. In: Large and Laguerie (Ed.), Fluidization VIII, Proceedings of the International Symposium of the Engineering Foundation. pp. 409–418.

Bear, J., Bachmat, Y., 1990. Introduction to Modelling of Transport Phenomena in Porous Media. Kluwer Academic Publishers, Dordrecht.

Ben-Dor, G., Levy, A., Sorek, S., 1997. Numerical investigation of the propagation of shock waves in rigid porous materials, Solution of the Riemann problem. International Journal of Numerical Methods for Heat and Fluid Flow 7 (8), 801–813.

Bortolozzi, R.A., Deiber, J.A., 2001. Comparison between two-and one-field models for natural convection in porous media. Chemical Engineering Science 56, 157–172.

Bussière, W., 2001. Influence of sand granulometry on electrical characteristics, temperature and electron density during high voltage fuse arc extinction. Journal of Physics D 34, 925–935.

Chen, Z., Lyons, S.L., Qin, G., 2001. Derivation of the Forchheimer law via homogenization. Transport in Porous Media 44, 325–335.

Courant, R., Friedrichs, K.O., 1948. Supersonic Flow and Shock Waves. Interscience Publishers Inc., New York.

De Ville, A., 1996. On the properties of compressible gas flow in a porous media. Transport in Porous Media 22, 287–306.

Hsieh, W.H., Lu, S.F., 2000. Heat-transfer analysis and thermal dispersion in thermally-developing region of a sintered porous metal channel. International Journal of Heat and Mass Transfer 43, 3001–3011.

Ishii, M., 1975. Thermo-fluid Dynamic Theory of Two Phase Flow. Eyrolles, Paris.

Jakubiuk, K., Lipski, T., 1993. Dynamics of fulgurite formation during arcing in HRC fuses. Journal of Physics D 26, 424–430.

Jiang, P.X., Ren, Z.P., 2001. Numerical investigation of forced convection heat transfer in porous media using a thermal non-equilibrium model. International Journal of Heat and Fluid Flow, 102–110.

Jiang, P.X., Ren, Z.P., Wang, B.X., 1999a. Numerical simulation of forced convection heat transfer in porous plate channels using thermal equilibrium or non-thermal equilibrium models. Numerical Heat Transfer (Part A) 35, 99–113.

Lee, D.Y., Vafai, K., 1999. Analytical characterization and conceptual assessment of solid and fluid temperature differentials in porous media. International Journal of Heat and Mass Transfer 42, 423–435.

Macdonald, I.F., El-Sayed, M.S., Mow, K., Dullien, F.A.L., 1979. Flow through porous media—the Ergun equation revisited. Ind. Eng. Fundam 18 (3).

Nield, D.A., 1994. Modelling high speed flow of a compressible fluid in a satured porous medium. Transport in Porous Media 14, 85–88.

Ochoa-Tapia, J.A., Whitaker, S., 1998. Heat transfer at the boundary between a porous medium and a homogeneous fluid: the one-equation model. Journal of Porous Media 1 (1), 31–46.

Rochette, D., Clain, S., 2003. Numerical simulation of Darcy and Forchheimer force distribution in a HBC fuse. Transport in Porous Media 53, 25–37.

Rochette, D., Clain, S., 2004. Mathematical model and simulation of gas flow through a porous medium in high breaking capacity fuses. International Journal of Heat and Fluid Flow 25, 115–126.

Roe, P.L., 1981. Approximate Riemann Solvers, Parameters Vectors and Difference Schemes. Journal of Computational Physics 43, 357–372.

Rohsenow, W.M., Hartnett, J.P., Cho, Y.I., 1998. Handbook of Heat Transfer. McGraw-Hill Handbooks, New York.

Simonin, O., 1991. Large eddy simulation applied to the motion of particules in stationary homogeneous fluid turbulence. In: Proceedings of 4th International Symposium on Gas–Solid Flows. ASME FED 121, p. 197.

Skjetne, E., Auriault, J.L., 1999. High-velocity laminar and turbulent flow in porous media. Transport in Porous Media 36, 131–147.

Sözen, M., Vafai, K., 1990. Analysis of the non-thermal equilibrium condensing flow of a gas through a packed bed. International Journal of Heat and Mass Transfer 33 (6), 1247–1261.

Teng, H., Zhao, T.S., 2000. An extension of Darcy's law to non-Stokes flow in porous media. Chemical Engineering Science 55, 2727–2735.

Toro, E.F., 1997. Riemann Solvers and Numerical Methods for Fluid Dynamics. Springer-Verlag, Berlin.

Touzani, R., Object Finite Element Library, Copyright ©1998–2003. Available from <http://www.lma.univ-bpclermont.fr/~touzani/ofeli.html>.

Vafai, K., Sözen, M., 1990a. Analysis of energy and momentum transport for fluid flow through a porous bed. Transactions of the ASME Journal of Heat Transfer 112, 690–699.

Vafai, K., Sözen, M., 1990b. An investigation of a latent heat storage porous bed and condensing flow through it. Transactions of the ASME Journal of Heat Transfer 112, 1014–1022.

Wakao, N., Kaguei, S., 1982. Heat and Mass Transfer in Packed Beds. Gordon and Breach Science, New York.

Whitaker, S., 1972. Forced convection heat transfer correlations for flow in pipes, past flat plates, single cylinders, single spheres, and for flow in packed beds and tube bundles. AIChe J. 18 (2), 361–371.

Whitaker, S., 1996. The Forchheimer equation: a theoretical development. Transport in Porous Media 25, 27–61.

Yee, H., 1987. Upwind and symmetric shock-capturing schemes. NASA Technical Memorandum 89464.